Quaternary Science Reviews 194 (2018) 1–11

Contents lists available at ScienceDirect

Quaternary Science Reviews

journal homepage: www.elsevier.com/locate/quascirev

Climate response of the Florida Peninsula to Heinrich events in the North Atlantic

T. Elliott Arnold [a, *], Aaron F. Diefendorf [b], Mark Brenner [a], Katherine H. Freeman [c], Allison A. Baczynski [c]

[a] Department of Geological Sciences, University of Florida, Gainesville, 32611, Florida, USA
[b] Department of Geology, PO Box 210013, University of Cincinnati, Cincinnati, 45221-0013, Ohio, USA
[c] Department of Geosciences, Pennsylvania State University, University Park, 16802, PA, USA

ARTICLE INFO

Article history:
Received 9 March 2018
Received in revised form
8 June 2018
Accepted 9 June 2018
Available online 26 June 2018

Keywords:
Heinrich events
Pleistocene
Paleoclimatology
North Atlantic
Hydrogen isotopes
Carbon isotopes
Biomarkers
Lake Tulane
Rapid climate change

ABSTRACT

Hydrogen and carbon isotope values (δD & $\delta^{13}C$) were measured on lipid biomarkers from a sediment core collected in Lake Tulane, Florida, USA, to infer shifts in climate and hydrologic variables during the Last Glacial. Isotopic trends from 24 samples correlate with plant community shifts evaluated in a previous pollen study by Grimm et al. (2006). We observe maxima in Δ_{leaf} values and minima in δD values concurrent with peaks in *Pinus* pollen abundances and Heinrich Events 4-2. Increased Δ_{leaf} values during North Atlantic cold spells indicate lower water-use-efficiency among angiosperms around Lake Tulane. Combined δD values from terrestrial and aquatic lipids, confirm that aridity decreased during cold, stadial periods (Heinrich Events), and increased during warm, interstadials. Furthermore, lower δD values in aquatic lipids during stadials are attributed to warming, as well as changing moisture sources. The anti-phase relationship between temperatures and aridity derived from our subtropical lacustrine record and those at high latitude in the North Atlantic is likely the result of complex ocean-atmosphere teleconnections that resulted from the collapse of Atlantic Meridional Overturning Circulation during Heinrich Events in the North Atlantic.

Published by Elsevier Ltd.

1. Introduction

Lake Tulane is a relatively small (~36 ha), deep (z_{max} ~25 m) solution lake located in south-central Florida, USA (Fig. 1). Its depth and location on a structural high, the Lake Wales Ridge, enabled continuous sediment accumulation since before the last glacial maximum. Palynological analysis of a sediment core from Lake Tulane indicated major shifts in plant communities over the past 60,000 years (Grimm et al., 1993). Of particular note are six peaks in *Pinus* (pine) pollen relative abundance, which coincide with the most intense cold phases of high-latitude Dansgaard–Oeschger (D-O) cycles and the Heinrich Events (HE) that terminated them. Alternating with *Pinus* peaks are zones with high relative percentages of *Quercus* (oak), *Ambrosia* (ragweed), *Lyonia* (staggerbush) and *Ceratiola* (rosemary) pollen, genera that today occupy the most xeric sites on the Florida landscape (Grimm et al., 2006). Additionally, the *Quercus* zones are replete with seeds from emergent aquatic plants, whereas all but one of the *Pinus* zones is devoid of macrofossils. Lack of emergent macrofossils in *Pinus* phases suggests that the lake was too deep to support emergent aquatic vegetation close to the core site. Based on the quantitative similarity of the Pleistocene *Pinus* zones with modern/Holocene Florida vegetation, the *Pinus* peaks, and therefore the HE, were interpreted as warm and wet periods in Florida, whereas the *Quercus* zones were inferred to have been drier, and likely colder than the *Pinus* zones.

The assertion that the *Pinus* phases, and HE, represent warm and wet periods in the subtropics is contentious. HE are recorded in the sediment record of the North Atlantic as layers of ice-rafted debris, lithic fragments from rocks of continental origin, which were derived from the calving and melting of large continental ice sheets (Bond et al., 1993). During Earth's last glacial interval, these episodic iceberg discharges perturbed global heat transport via reduction in the Atlantic meridional overturning circulation (AMOC) (Lynch-Stieglitz et al., 2014). Although the mechanism responsible for

* Corresponding author. Department of Geology and Environmental Science, University of Pittsburgh, Pittsburgh, 15260, Pennsylvania, USA.
E-mail address: tea27@pitt.edu (T.E. Arnold).

https://doi.org/10.1016/j.quascirev.2018.06.012
0277-3791/Published by Elsevier Ltd.

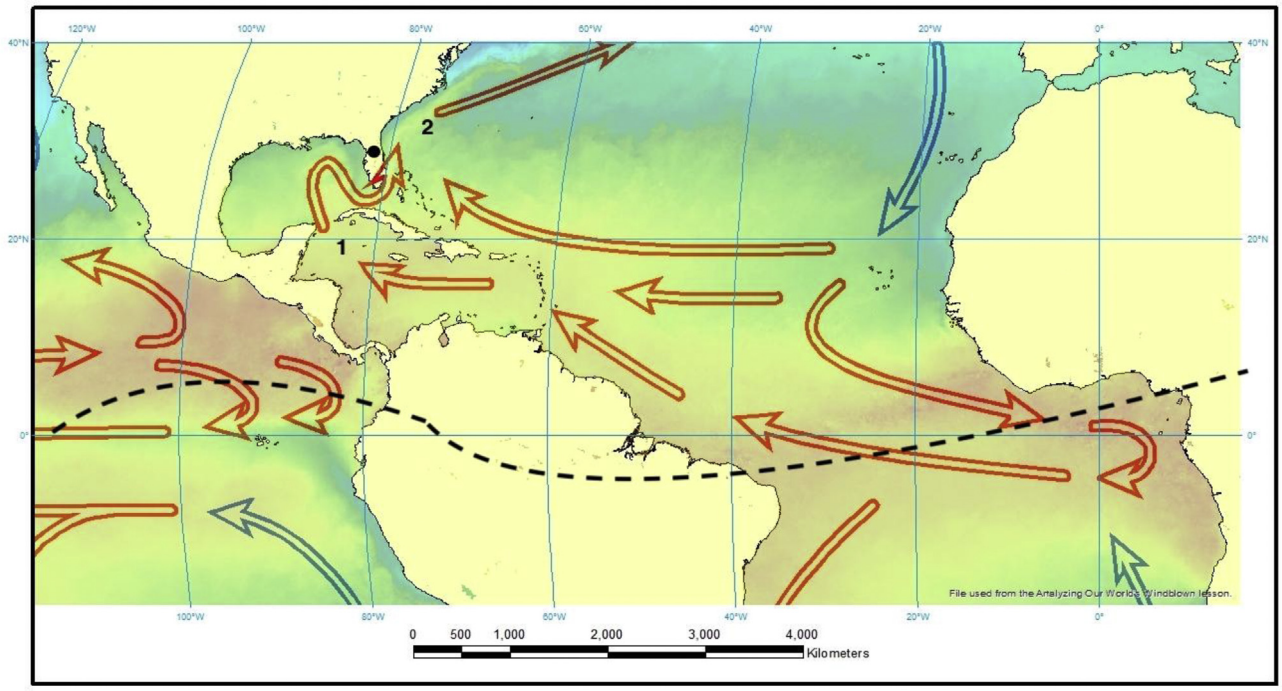

Fig. 1. Sea-surface temperatures and major surface ocean currents (warmer surface water in red, cooler surface water in blue). Location of Lake Tulane (black dot), the Loop Current (1), Gulf Stream (2), and the approximate location of the Inter-Tropical Convergence Zone (dashed line) during the boreal winter. The Atlantic Warm pool is the area of high temperatures (red colors) in and around the Gulf of Mexico and the Caribbean. (For interpretation of the references to colour in this figure legend, the reader is referred to the Web version of this article.)

these events is still debated (Hemming, 2004; Marcott et al., 2011), teleconnections between HE and rapid climate oscillations have been recorded globally (Broecker, 2006). Their occurrence at the end of progressively cooler Greenland D-O interstadial cycles has led to the conclusion that HE were synchronous with lower temperatures and increased aridity over large regions of the Northern Hemisphere (Broecker et al., 1992; Zhao et al., 2003; Zhou et al., 2008). This hypothesis is supported by numerous lines of evidence, including Iberian Margin sea-surface-temperature (SST) reconstructions derived from Mg/Ca ratios (Patton et al., 2011) and alkenone $U^{K'}_{37}$ records (Pailler and Bard, 2002), the relative abundance of the polar planktonic foraminiferan *Neogloboquadrina pachyderma* (sinistral) in the western Mediterranean (Cacho et al., 1999), and $\delta^{18}O$ records from marine sediment cores in the Icelandic and Irminger Seas (Kreveld et al., 2000).

Although these studies indicated an in-phase relationship between SST and climate conditions in Greenland, there appears to be an anti-phase tendency in numerous other climate reconstructions, in particular, those from low to middle latitudes in the Atlantic (Hemming, 2004). Alkenone-based temperature reconstructions from the southernmost portions of the ice-rafted debris belt (40–55°) indicate that surface waters were 2–4 °C warmer during all six Heinrich Events (Naafs et al., 2013). Farther south in the western Atlantic, temperatures approached modern values during HE1 (Weldeab et al., 2006; Carlson et al., 2008) and HE5a (Schmidt et al., 2006), implying warm surface waters prior to transitions into interstadials. These results are in line with late-glacial circulation models, which produce warmer and more saline waters in middle latitudes of the western Atlantic when AMOC strength is at its minimum, prior to the onset of HE farther north (Renold et al., 2010).

Reduced northward transport of heat just before and during HE could be the source of the subtropical warming, hypothesized by Grimm et al. (2006) to be a prerequisite for *Pinus* proliferation. This idea was corroborated by coupled climate model simulations (Weaver et al., 2003) and pollen-climate inference models specific to Florida (Donders et al., 2011). Results from these modeling experiments demonstrate that a decrease in SST in the North Atlantic would increase the meridional temperature gradient, strengthen the trade winds and expand the Atlantic Warm Pool, resulting in more precipitation across the Florida Peninsula during HE (Donders et al., 2011).

Despite the results of modeling experiments, there are few empirical terrestrial records that document changes in temperature and precipitation across stadial/interstadial boundaries. In fact, the palynological studies from subtropical Lake Tulane represent the primary archive for terrestrial changes associated with HE in North America (Grimm et al., 1993, 2006). Shortcomings of pollen reconstructions, however, which include inter-species differences in pollen production, dispersal, and preservation, make sedimentary pollen records potentially equivocal with respect to their ability to provide an accurate characterization of regional plant communities (Bennet and Willis, 2002). Furthermore, pollen of different species within the genera *Pinus* and *Quercus* cannot be distinguished. Today, taxa within each genus occupy different habitats across Florida's effective moisture gradient, and this complicates assignment of plant genera to wet or dry environments. Given the lack of terrestrial records associated with HE, and potential problems associated with palynological reconstructions, additional lines of evidence are needed to test hypotheses regarding climate changes at low latitudes during HE.

1.1. Carbon isotopes and precipitation

Carbon isotope ratios ($\delta^{13}C$) of plant leaf waxes (*n*-alkanes) in lake sediment cores have been used to infer shifts in precipitation and aridity over geologic timescales (e.g., Magill et al., 2013). Variations in the carbon isotopic composition of leaf waxes, are caused

by changes in precipitation (wetter/drier periods) and plant community abundances. In regions and biomes with higher mean annual precipitation (MAP), greater ^{13}C discrimination by C_3 plants is expected and results in more negative leaf wax $\delta^{13}C$ values (e.g., Diefendorf et al., 2010; Kohn, 2010; Diefendorf and Freimuth, 2017). Mixing of *n*-alkanes chain-lengths from different plant communities can also raise or lower $\delta^{13}C$ values depending on their respective biosynthetic fractionation values. Of the dominant pollen types measured in the Lake Tulane core, only *Quercus* and *Ambrosia* produce significant quantities of *n*-C_{29} and *n*-C_{31} alkanes (Diefendorf et al., 2015). Therefore, in the Lake Tulane sediment record, shifts in $\delta^{13}C$ values of *n*-alkanes are primarily driven by aridity differences and mixing of plant communities with different biosynthetic fractionation values.

The association between aridity (or decreased precipitation), and more positive $\delta^{13}C_{leaf}$ values has been observed in many studies, with isotopic variability exceeding 6‰ among plant communities across rainfall gradients (Ehleringer and Cooper, 1988; Stewart et al., 1995; Hartman and Danin, 2010). Measurements from a single *Pinus* species showed a ~2‰ decrease in $\delta^{13}C_{leaf}$ values across a 400 mm gradient of increasing precipitation in northeastern Spain (Ferrio et al., 2003), and values increased by ~3‰ in water deficit treatments (Waghorn et al., 2015). Taken together, these studies indicate that, once corrected for changes in $\delta^{13}C_{atmosphere}$ and carbon isotope discrimination (or Δ_{leaf}, Eq. (2)) is primarily driven by water availability (Diefendorf et al., 2010).

1.2. Hydrogen isotopes and precipitation

A strong positive correlation between δD ratios of terrestrial plant lipids and δD ratios of weighted mean annual precipitation has been demonstrated by various investigations (Sachse et al., 2010, 2012; Polissar and Freeman, 2010). Other studies have documented additional climatological (precipitation sources and patterns), physiological (species-related photosynthetic offsets), or hydrological (precipitation amount) effects on δD values of leaf waxes (δD_{lipid}). Chief among these effects is D-enrichment of leaf water resulting from evapotranspiration, which is primarily driven by relative humidity (Kahmen et al., 2008, 2013a; b).

Studies of leaf wax hydrogen isotope variability measured across precipitation gradients indicate that δD_{lipid} values are significantly enriched by transpiration in more arid environments (Smith and Freeman, 2006; Douglas et al., 2012). A study of *n*-alkanes from field-grown barley (*Hordeum vulgare*) showed that relative humidity influenced δD_{lipid} values, suggesting that the hydrogen isotopic composition of leaf waxes yields a record of precipitation that is strongly modified by leaf water evaporation (Sachse et al., 2010). This effect is recorded in numerous other δD records that display decreased isotopic fractionation in lipids in sediments from arid sites (Polissar and Freeman, 2010), and among *n*-alkanes from plants across aridity gradients (Feakins and Sessions, 2010).

Thus, Δ_{leaf} and δD_{lipid} values in lake sediments should serve as indicators of past aridity and these tools can be used to evaluate changes in Florida climate during HE. For example, during the hypothesized wet *Pinus* phases, Δ_{leaf} should be higher and δD_{lipid} values should be relatively lower, whereas during the dry *Quercus* periods, Δ_{leaf} should be lower and δD_{lipid} ratios relatively higher. In this study, we inferred temperature and precipitation changes across three HE (2-4) using the isotopic values (Δ_{leaf} and δD) of *n*-alkanes extracted from the same sediment core from Lake Tulane that Grimm et al. (2006) used to develop their pollen record. We hypothesize that precipitation in Florida was relatively greater during HE because of low-latitude warming associated with reduced AMOC strength.

2. Materials and methods

2.1. Study site and sample collection

Lake Tulane (Latitude 27°35′9″N; Longitude 81°30′13″W) occupies a surficial-groundwater-fed solution basin on the Lake Wales Ridge, an elongated, relict coastal ridge that has been above sea level since the early Pliocene (White, 1970). The sediments on the ridge are composed of coarse-grained quartz sands and gravels, often bound together with clays of fluvial origin (White, 1970). Lake Tulane is a relatively deep (z_{max} ~25 m), oligotrophic water body (total phosphorus = 6 μg/L; Chl *a* = 3 μg/L) that is hydrologically isolated from the deep, Eocene-age limestone Floridan Aquifer, but receives seepage input through the shallow surficial aquifer. In spite of low aquatic productivity, the lake sediments are organic-rich (>10% organic matter). Despite its location above a limestone platform, the lake deposits lack carbonate.

A total of 24 sediment samples, four from each *Pinus* zone 2-4 (TP 2-4) and *Quercus* zone 6-8 (TQ 6-8), were taken from the core retrieved by Grimm et al. (2006) at 8–10 cm intervals. The core chronology is based on 55 Accelerator Mass Spectrometry (AMS) dates on bulk sediments and, where available, terrestrial macrofossils. Our sampled interval (40,000–17,000 yr BP) fell within the range of radiocarbon dating. Grimm et al. (2006) calibrated samples < 20,000 ^{14}C yr BP using CALIB 5.0.2 with the INTCAL04 calibration curve, and for samples dated to 20,000–40,000 ^{14}C yr BP, the Fairbanks0805 calibration curve was applied (Fairbanks et al., 2005). See Grimm et al. (2006) for further details on calibration of the AMS dates.

2.2. Lipid extraction, purification and quantification

Sediment samples were freeze-dried and lipids were extracted with an Accelerated Solvent Extractor ASE200 (Dionex), using 2:1 (v/v) dichloromethane (DCM):methanol through three extraction cycles at 10.3 MPa (1500 psi) and 100 °C. Between 1 and 2 g of sediment were used for lipid extraction. Total lipid extracts (TLE) were concentrated under a gentle stream of nitrogen, and the neutral lipid fraction was obtained after base saponification of the TLE. Neutral lipids were further separated, based on polarity, into compound classes by column chromatography, using 5% deactivated silica gel, according to methods modified from Nichols (2011). Hydrocarbons were eluted from the silica gel column with 4.5 mL of 9:1 Hexane:DCM, and saturated hydrocarbons were separated from alkenes on 5% Ag-impregnated silica gel (w/w) with 4 mL of hexane and ethyl acetate, respectively.

A Thermo Scientific Trace 1310 gas chromatograph with a fused silica capillary column (Agilent J&W DB-5; 30 m long, 0.32 mm I.D., 0.25 μm film thickness), interfaced to a Thermo Scientific TSQ 8000 triple quadrupole mass spectrometer with electron ionization, was used for compound identification. The split/splitless inlet was operated in splitless mode at 300 °C with helium as the carrier gas. The column flow rate was 2.0 mL/min and the oven was held at an initial temperature of 60 °C for 1 min, then ramped to 140 °C at 15 °C/min, and to 320 °C at 4 °C/min and held for 25 min *n*-Alkane quantification was carried out on a Thermo Scientific Trace 1310 GC fitted with a flame ionization detector (GC-FID), using the same oven program as above. Androstane was added to sample vials prior to injection for use as an internal standard to estimate percent recovery. Quantification was based on calibration curves generated from the peak areas of external standards (C_7-C_{40}) with concentrations ranging from 5 to 250 μg/mL.

2.3. Compound-specific isotope measurements

Compound-specific $\delta^{13}C$ values were measured at Pennsylvania State University using a gas chromatograph coupled to an isotope ratio mass spectrometer (IRMS) interfaced with a GC-C combustion system. The *n*-alkanes were separated on a Varian model 3400 GC with a split/splitless injector operated in splitless mode. A fused silica capillary column (Agilent J&W DB-5; 30 m long, 0.32 mm I.D., 0.25 μm film thickness) was used with helium as the carrier gas and a column flow rate of 2.0 mL/min. The oven program began at a temperature of 60 °C, was held for 1 min, then increased at a rate of 6 °C/min to 320 °C, which was held for 20 min. Following GC separation, *n*-alkanes were combusted over nickel-platinum wire with O_2 in He (1%, v/v) at 1000 °C. Isotope ratios of carbon in CO_2 were measured using a Finnigan Mat 252 isotope ratio mass spectrometer. Isotopic abundances were determined relative to a reference gas calibrated with Mix B (*n*-C_{16} to *n*-C_{30}; Arndt Schimmelmann, Indiana University). Carbon isotope values of samples were normalized to the VPDB scale using the Uncertainty Calculator (Polissar and D'Andrea, 2014) and are reported in standard delta notation as follows:

$$\delta^{13}C = [(({}^{13}C/{}^{12}C)_{\text{sample}}/({}^{13}C/{}^{12}C)_{\text{standard}}) - 1] \times 1000 \quad (1)$$

Standard errors of the mean (SE) were calculated using the Uncertainty Calculator, which yielded a 1σ SE value of ±0.36‰ (Polissar and D'Andrea, 2014).

To eliminate possible confounding results associated with past changes in $\delta^{13}C$ values of atmospheric CO_2, all carbon isotope data are presented as Δ_{leaf} values (Farquhar et al., 1989), where:

$$\Delta_{leaf} = (\delta^{13}C_{atm} - \delta^{13}C_{leaf})/(1 + \delta^{13}C_{leaf}/1000) \quad (2)$$

Leaf $\delta^{13}C$ values ($\delta^{13}C_{leaf}$) were calculated from *n*-alkane $\delta^{13}C$ values where:

$$\delta^{13}C_{leaf} = (1000 + \delta^{13}C_{alkane})/((\varepsilon_{lipid/leaf}/1000) + 1)) - 1000 \quad (3)$$

Carbon isotope values for atmospheric CO_2 were taken from Leuenberger et al. (1992) and data were interpolated using a cubic spline. Carbon isotope values of atmospheric CO_2 ranged from −6.3‰ to −7.1‰ across the studied interval. By accounting for variations in carbon source, the Δ_{leaf} value primarily becomes a signal for changes in water availability and plant community (Diefendorf et al., 2010). $\varepsilon_{lipid/leaf}$ values are from Diefendorf and Freimuth (2017) and are shown in Table 2. Mean values (with 1σ standard deviations) for each chain length are as follows: *n*-C_{23} = −3.2‰ (2.1‰), *n*-C_{27} = −4.1‰ (1.6‰), *n*-C_{29} = −4.6‰ (2.2‰), *n*-C_3 = −5.1‰ (2.2‰), *n*-C_{33} = −5.8‰ (1.8‰), *n*-C_{35} = −6.1‰ (4.0‰).

Compound-specific hydrogen isotopes were measured at the University of Cincinnati using a Thermo Trace GC Ultra coupled to a Thermo Electron Delta V Advantage IRMS with an Isolink combustion furnace. A fused silica capillary column (Agilent J&W DB-5; 30 m long, 0.25 mm I.D., 0.25 μm film thickness) was used with helium as the carrier gas and a column flow rate of 1.5 mL/min using a split/splitless injector operated in splitless mode. The oven program was slightly modified from the schedule above: 80 °C (2 min), then to 320 °C (held 10 min) at 8 °C/min. Hydrogen isotope abundances and standard errors were calculated as described above for carbon isotopes. Reference gas values were calibrated with Mix A (*n*-C_{16} to *n*-C_{30}; Arndt Schimmelmann, Indiana University). The H_3^+ factor had a mean value of 6.2. Calculation of isotope abundances and correction of δD values to the Vienna Standard Mean Ocean Water (VSMOW) scale was carried out in the same way as for carbon isotopes, and the pooled 1σ SE for all samples was ±3.2‰ (Polissar and D'Andrea, 2014). Hydrogen isotope values are reported in standard delta notation relative to VSMOW as follows:

$$\delta D = [((D/H)_{\text{sample}}/(D/H)_{\text{standard}}) - 1] \times 1000 \quad (4)$$

2.4. Calculating variations in aridity using $\varepsilon_{(terr\text{-}aq)}$

Changes in evapotranspiration have been qualitatively measured as the difference between terrestrial and aquatic lipid δD values (Jacob et al., 2007; Rach et al., 2014, 2017). We estimate changes in evapotranspiration by first calculating the apparent fractionation factor (α) between terrestrial (*n*-C_{29}) and aquatic lipids (*n*-C_{23}) as:

$$\alpha = (1000 + \delta D_{n\text{-}C29})/(1000 + \delta D_{n\text{-}C23}) \quad (5)$$

Then converting the apparent fractionation to epsilon notation in units of permil (‰) as follows:

$$\varepsilon_{(terr\text{-}aq)} = (\alpha - 1)1000 \quad (6)$$

The primary assumptions of this approach are outlined in Rach et al. (2017). Briefly, we make two major assumptions: 1) δD values of aquatic lipids equal the δD values of mean annual precipitation, and 2) biosynthetic fractionation values of terrestrial and aquatic lipids remained constant throughout the Lake Tulane record. Lake Tulane's waters are only moderately affected by evaporative enrichment because of the relatively large volume of the lake and the moderating effect of continuous shallow groundwater inputs. This is supported by data from a recent study that tracked $\delta^{18}O$ in the Lake Tulane water column over a three-year period (Escobar et al., 2009). During that time, the average intra-annual variability in $\delta^{18}O$ was 0.6‰, which translates into a change of ~5‰ in δD, using the local meteoric water line relationship as a first estimate (Florea and McGee, 2010). We assumed that annual evaporative enrichment of lake waters during the Pleistocene was similar to that today and had minimal influence on the isotope values of lake water. Changes in δD values of aquatic lipids, therefore, reflect changes in mean annual precipitation. Biosynthetic fractionation values are discussed at length below, but based on vegetation reconstructions from palynological (Grimm et al., 1993, 2006) and isotopic data (Huang et al., 2006; Diefendorf et al., 2015), we conclude that the terrestrial *n*-alkane record (i.e. *n*-C_{29}) is dominated by C_3 angiosperms (primarily *Quercus*) and the aquatic *n*-alkane record (i.e. *n*-C_{23}) is a mixture of submerged aquatic vegetation with major contributions from *Potamogeton*. The biosynthetic fractionation values of these plant genera did not likely change throughout our sediment record. As such, terrestrial leaf water evaporative enrichment can therefore be calculated using $\varepsilon_{(terr\text{-}aq)}$ (Eq. (6)).

3. Results

3.1. n-Alkane concentrations and chain length distributions

Concentrations of select *n*-alkane chain lengths are provided in Fig. 2. The *n*-alkane chain lengths are dominated by the long-chain alkanes (i.e., > *n*-C_{25}), with *n*-C_{29} displaying the highest average abundance (120.3 μg/g OC) throughout the Lake Tulane sediment record. We calculated the average chain length (ACL) for all samples using the Eglinton and Hamilton (1967) equation, as reported in

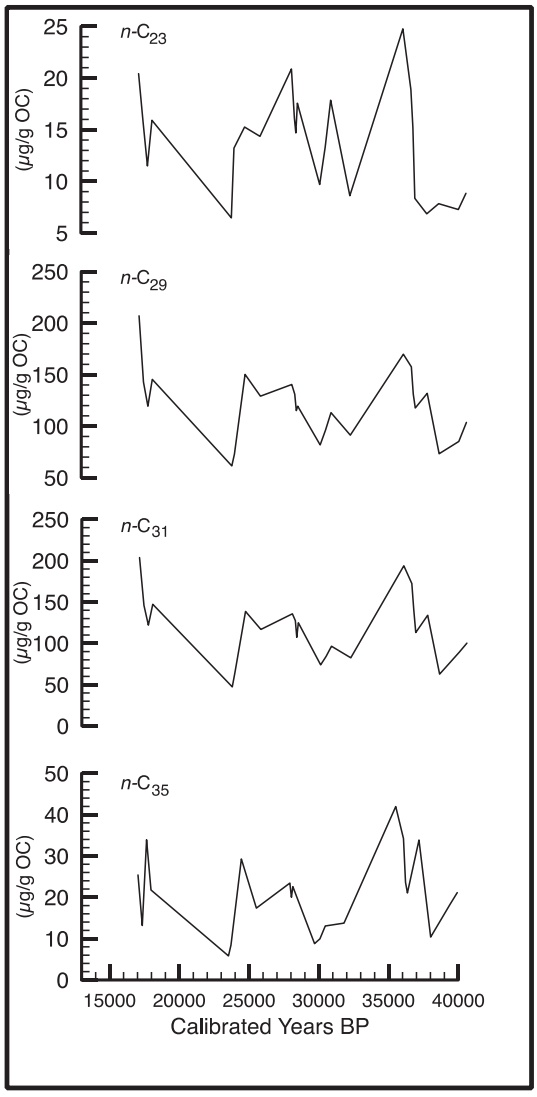

Fig. 2. Concentrations of select *n*-alkane chain lengths. Note scales differences on the y-axes.

Diefendorf and Freimuth (2017):

$$\mathrm{ACL(C25-C35)} = \frac{25C_{25}+27C_{27}+29C_{29}+31C_{31}+33C_{33}+35C_{35}}{C_{25}+C_{27}+C_{29}+C_{31}+C_{33}+C_{35}} \quad (7)$$

There is low variability in ACL throughout the record. The highest ACL value is 30.1 and the lowest is 29.2, with a mean ACL of 29.7 for the entire record (Table 1). Carbon preference index (CPI) values were calculated from the equation of Marzi et al. (1993):

$$\mathrm{CPI} = 0.5\,\frac{C_{21}+C_{23}+C_{25}+C_{27}\ldots+C_{33}}{C_{22}+C_{24}+C_{26}+C_{28}\ldots+C_{32}} \quad (8)$$

The *n*-alkane CPI values for all samples are >1, and exhibit a strong odd over even predominance, which indicates higher odd-chain *n*-alkane abundances. CPI values range from a minimum of 2.0 and a maximum of 3.2, with an average of 2.7 (Table 1).

Differences in mean *n*-alkane concentrations are apparent between *Pinus* and *Quercus* phases. Highest average abundances for carbon chain lengths *n*-C_{27}-C_{35} occurred during *Quercus* phases. *n*-Alkanes derived from C_3 dicots (*n*-C_{27} and *n*-C_{29}) increased in average abundance by 75% (*n*-C_{27}) and 70% (*n*-C_{29}) during the *Quercus* intervals. Furthermore, *n*-alkane biomarkers from mixed C_3/C_4 sources, *n*-C_{33} and *n*-C_{35}, increased by 64% and 62%, respectively, during the *Quercus* intervals. Abundances of *n*-C_{23}, typically the most common *n*-alkane chain length in submerged aquatic plants and less abundant in terrestrial plants (Ficken et al., 2000; Aichner et al., 2010a; Diefendorf et al., 2011; Diefendorf and Freimuth, 2017), were higher during *Quercus* phases by ~60%.

Table 1
Values for the carbon preference index (CPI) and average chain length (ACL) in the Lake Tulane core. The ages are calibrated following the methods outlined in Grimm et al. (2006), and the phases are Tulane *Quercus* (TQ) and Tulane *Pinus* (TP), which are also described in the Grimm et al. (2006) paper.

Age (cal. Yrs BP)	CPI	$ACL_{25\text{-}35}$	Phase
17038	3.21	29.64	TQ6
17345	2.97	29.54	TQ6
17655	0.84	29.94	TQ6
17965	2.04	29.73	TQ6
23522	2.75	29.23	TP2
23706	2.77	29.23	TP2
24447	2.81	29.69	TP2
25519	2.67	29.44	TP2
27716	2.63	29.48	TQ7
27925	2.90	29.63	TQ7
28030	2.89	29.64	TQ7
28134	2.76	29.68	TQ7
29693	3.09	29.55	TP3
30075	2.85	29.36	TP3
30457	2.93	29.31	TP3
31804	3.04	29.51	TP3
35511	2.27	30.00	TQ8
36068	2.35	30.04	TQ8
36207	2.33	29.93	TQ8
36347	2.71	29.84	TQ8
37180	2.38	30.13	TP4
38014	2.62	29.50	TP4
39386	2.66	29.96	TP4
39923	3.11	29.82	TP4

3.2. Carbon isotope results

The Δ_{leaf} values for carbon chain lengths *n*-C_{27}-C_{35} are shown in Fig. 3 and mean Δ_{leaf} values for all chain lengths are provided in Table 2. The *n*-alkanes with 31, 33, and 35 carbon atoms displayed the greatest range in Δ_{leaf} values: 2.7‰ (max = 21.4‰, min = 18.7‰), 5.7‰ (max = 24.3‰, min = 18.6‰), and 4.7‰ (max = 21.3‰, min = 16.6‰), respectively, whereas the range in Δ_{leaf} values of *n*-alkanes with 27 and 29 carbons was 1.7‰ (max = 22.4‰, min = 20.7‰) and 2.0‰ (max = 21.9‰, min = 19.9‰), respectively. Correlations between Δ_{leaf} values and *Pinus* pollen percentages (which coincide with Greenland stadial periods) are greater for chain lengths *n*-C_{27} ($r = 0.62$, $n = 24$, $p < 0.001$), *n*-C_{29} ($r = 0.54$, $n = 24$, $p < 0.01$), and *n*-C_{35} ($r = 0.58$, $n = 24$, $p < 0.01$), than for chain lengths *n*-C_{31} ($r = 0.44$, $n = 24$, $p < 0.05$) and *n*-C_{33} ($r = 0.40$, $n = 24$, $p < 0.05$). Mean Δ_{leaf} values for

Table 2
Δ_{leaf} values (all in ‰) for select *n*-alkane chain lengths extracted from the Lake Tulane core and atmospheric $\delta^{13}C$ ($\delta^{13}C_{atms}$) values taken from Leuenberger et al. (1992). Δ-leaf values were calculated using the following $\varepsilon_{lipid/leaf}$ values (from Diefendorf and Freimuth, 2017): *n*-$C_{23} = -3.2$‰, *n*-$C_{27} = -4.1$‰, *n*-$C_{29} = -4.6$‰, *n*-$C_{31} = -5.1$‰, *n*-$C_{33} = -5.8$‰, *n*-$C_{35} = -6.1$‰.

Age (cal yr BP)	C_{23} Δ-leaf	C_{27} Δ-leaf	C_{29} Δ-leaf	C_{31} Δ-leaf	C_{33} Δ-leaf	C_{35} Δ-leaf	$\delta^{13}C$- atm	Phase
17,038	23.7	22.1	21.3	20.7	23.0	19.1	−6.5	TQ6
17,345	21.6	20.6	20.0	19.2	19.8	16.6	−6.4	TQ6
17,655	23.8	21.6	20.7	19.5	19.3	17.1	−6.4	TQ6
17,965	23.6	21.2	20.3	19.6	18.7	17.3	−6.3	TQ6
23,522	n/a	22.3	21.0	20.1	20.2	20.1	−6.9	TP2
23,706	22.5	21.0	20.4	19.4	18.6	n/a	−6.7	TP2
24,447	22.5	22.1	21.0	20.1	19.4	18.8	−6.5	TP2
25,519	22.3	22.0	20.8	20.2	19.5	18.6	−6.4	TP2
27,716	21.1	21.4	20.7	20.0	21.4	18.9	−6.8	TQ7
27,925	21.9	20.8	19.9	19.5	19.7	18.4	−6.9	TQ7
28,030	22.5	21.4	20.5	19.7	20.3	18.5	−6.9	TQ7
28,134	21.5	21.2	20.8	20.1	20.5	17.9	−6.7	TQ7
29,693	n/a	21.5	20.7	19.7	21.5	n/a	−6.5	TP3
30,075	24.5	22.4	21.3	21.4	21.4	n/a	−6.4	TP3
30,457	24.4	21.9	20.8	20.0	22.0	n/a	−6.4	TP3
31,804	23.0	20.8	20.2	18.7	20.6	n/a	−6.5	TP3
35,511	21.0	21.2	20.5	20.2	19.5	17.8	−7.0	TQ8
36,068	21.2	21.4	20.9	20.3	21.3	19.5	−7.1	TQ8
36,207	20.9	21.2	20.6	19.8	20.8	19.4	−7.1	TQ8
36,347	21.3	21.2	20.7	19.8	20.4	19.1	−7.1	TQ8
37,180	n/a	22.3	20.9	20.3	24.3	20.6	−6.7	TP4
38,014	21.9	21.7	21.2	21.1	22.5	18.6	−6.4	TP4
39,386	22.8	22.2	21.9	21.4	23.8	21.3	−6.3	TP4
39,923	21.8	21.7	21.6	20.6	22.5	19.8	−6.3	TP4

Pinus zones were an average of 0.8‰ greater than means for *Quercus* zones.

3.3. Hydrogen isotope results

The hydrogen isotopic compositions for select *n*-alkanes are displayed in Fig. 3 and Table 3. As with carbon isotope results, *n*-alkanes with 33 and 35 carbon atoms (*n*-$C_{33} = 32$‰, *n*-$C_{35} = 25$‰) exhibited a greater range in δD values compared to *n*-alkanes with 27 and 29 carbon atoms (*n*-$C_{27} = 20$‰, *n*-$C_{29} = 21$‰). The largest range in δD values was found in alkane *n*-C_{23} (43‰). For all chain lengths, the mean δD value is higher during *Pinus* phases and lower during the *Quercus* zones. The greatest difference between means was recorded in the *n*-C_{23} alkane (19‰), and all other chain lengths displayed differences in means (*Pinus*-*Quercus*) ranging from 2.6 to 8.2‰. Hydrogen isotope values begin to decrease prior to the end of each *Pinus* phase. As a result, δD profiles for all but one chain length (*n*-C_{23}) are not significantly correlated with *Pinus* pollen percentages (Fig. 3).

To estimate Pleistocene lake water values (δD_{lake}) and terrestrial leaf water deuterium enrichment (δD_{terr}), we first had to calculate $\varepsilon_{l/w}$ values, or apparent biosynthetic fractionation between lipid and source water, defined as $[((D/H)_{lipid}/(D/H)_{water}) - 1]$, for *n*-alkanes from different plant communities. Aquatic macrophyte $\varepsilon_{l/w}$ values were taken from Aichner et al. (2010b), who calculated the average biosynthetic offset between the C_{23} *n*-alkane from the submerged macrophyte *Potamogeton* and Tibetan lake water to be −82‰. We note that Grimm et al. (2006) identified *Potamogeton* macrofossils in the Lake Tulane core and the genus is currently found throughout Florida lakes. The $\varepsilon_{l/w}$ values for terrestrial plants in this study were taken from Freimuth et al. (2017), who calculated an average $\varepsilon_{l/w}$ value of -135 ± 11‰ from measurements on *Q. alba* plants from the Midwest United States. This value is similar to other $\varepsilon_{l/w}$ calculations from temperate deciduous forests of Pennsylvania (−131‰, Polissar and Freeman, 2010), and from lake sediments in angiosperm dominated European watersheds (−133‰, Sachse et al., 2004).

Here, we found that ($\varepsilon_{(terr\text{-}aq)}$) values had a mean of −14.5‰ and a range of 35‰. Higher values are indicative of greater aridity. Overall, $\varepsilon_{(terr\text{-}aq)}$ is negatively correlated with percent *Pinus* pollen ($r = -0.80$, $n = 21$, $p < 0.001$), with $\varepsilon_{(terr\text{-}aq)}$ values, on average, 17‰ higher during *Quercus* phases (Fig. 4).

4. Discussion

4.1. Reconstructing paleohydrology from leaf wax carbon and hydrogen isotopes

The late Pleistocene was characterized by periods of rapid climate fluctuations brought about by changes in ocean circulation and ice volume. These climate events have been studied extensively in sediment records from marine sites in the high-latitude north Atlantic, but rarely have they been documented in subtropical terrestrial sites. Both carbon and hydrogen isotope ratios preserved in Lake Tulane's *n*-alkanes record respond to changes in water availability, therefore vegetation transitions from *Pinus*-dominated to *Quercus*-dominated phases should have produced measurable differences in leaf wax carbon and hydrogen isotopes.

Across the study interval, variations in the concentration and isotopic signature of atmospheric carbon dioxide are small and would not affect carbon isotope fractionation (Schubert and Jahren, 2012; Eggleston et al., 2016). Therefore, the Δ_{leaf} value is primarily a function of precipitation amount, with low Δ_{leaf} indicative of lower precipitation and lower stomatal conductance (Diefendorf et al., 2010; Kohn, 2010). Although our ranges in Δ_{leaf} values are small, they are correlated with changes in *Pinus* abundance. For example, *n*-C_{29} Δ_{leaf} values are positively correlated ($r = 0.54$, $p < 0.01$) with changes in the relative abundance of *Pinus* pollen. At this site, changes in the relative abundance of *Pinus* pollen have been previously interpreted as changes in water availability (Grimm et al., 2006).

The range (2‰) in *n*-C_{29} Δ_{leaf} values between *Pinus* and *Quercus* phases is in line with $\delta^{13}C$ ranges (~2‰) measured in modern experiments with a single taxon, during which *Pinus halepensis* received different amounts of water (Ferrio et al., 2003), and with natural variability among woody perennial plants (~3‰) that were

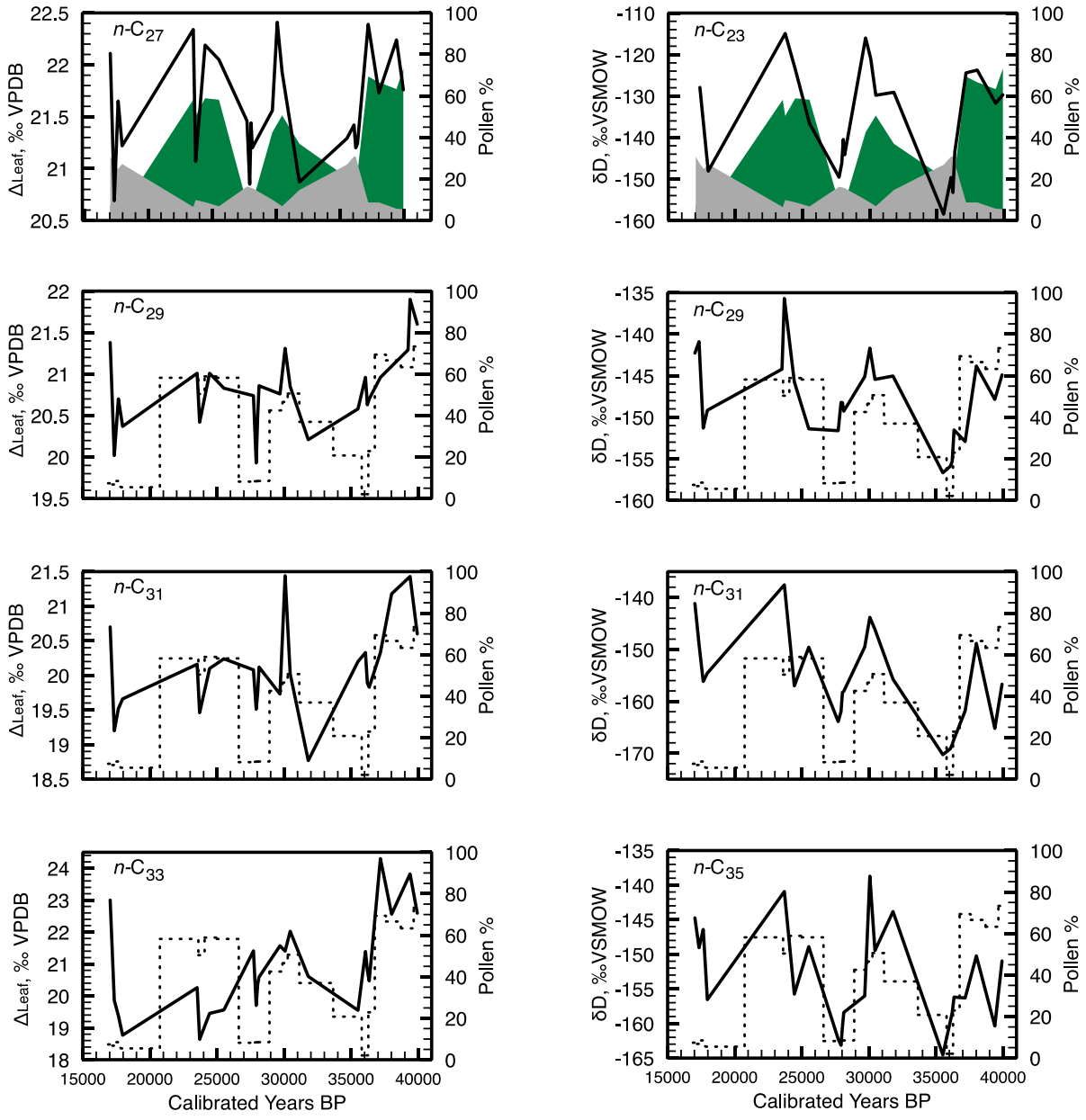

Fig. 3. Select Δ_{leaf} values (left panel) and their δD values (right panel) for different *n*-alkane chain lengths. Percent abundance of *Pinus* pollen in green and *Quercus* pollen in grey are displayed in the top graph of each panel. Dashed lines in subsequent graphs indicate *Pinus* pollen abundances. All Δ_{leaf} values have a 1σ SE value of ±0.35‰, and the pooled 1σ SE for all δD samples was ±3.2‰. (For interpretation of the references to colour in this figure legend, the reader is referred to the Web version of this article.)

sampled across rainfall gradients in the Mediterranean (Hartman and Danin, 2010). Based on the similarity in carbon isotope fractionation values between sedimentary and modern growth experiments, we infer from higher Δ_{leaf} values during *Pinus* phases that precipitation and carbon isotope discrimination increased among terrestrial vegetation.

A portion of the 2‰ variability in the *n*-C_{29} Δ_{leaf} profile could be the result of mixing of *n*-alkanes from different plant communities. It is unlikely that C_3 gymnosperms are the source of this variability, as research on chain-length distributions among terrestrial vegetation shows that most North American gymnosperms (i.e. *Pinaceae*) produce very low concentrations of *n*-alkanes relative to angiosperms (Diefendorf et al., 2011, 2015). Additionally, contributions from C_4 grasses can also be ruled out as previous biomarker and pollen research on the same sediment core from Lake Tulane demonstrated that C_4 contributions to the organic carbon pool dropped from ~50% during *Quercus* phases to nearly 0% during *Pinus* phases (Grimm et al., 2006; Huang et al., 2006). These results are in agreement with our *n*-alkane concentration data, which record a ~60% drop in *n*-C_{33} and *n*-C_{35} in *Pinus* zones (Fig. 2). The behavior of *n*-$C_{33/35}$ in the record is likely related to plant physiology: C_4 graminoids contain *n*-C_{33} (Wang et al., 2013; Garcin et al., 2014) and *n*-C_{35} (Diefendorf and Freimuth, 2017) alkanes in their leaves at concentrations an order of magnitude greater than in woody C_3 angiosperms, and *n*-C_{29} concentrations that are 75% less than in C_3 angiosperm trees (Diefendorf and Freimuth, 2017). From this, we infer no graminoid contribution to the *n*-C_{29} record during *Pinus* zones, and a negligible contribution of *n*-C_{29} from C_4 grasses

Table 3
δD values (all in ‰) for select *n*-alkane chain lengths extracted from the Lake Tulane core. Core phases are as follows: Tulane *Pinus* (TP), and Tulane *Quercus* (TQ).

Age (cal yr BP)	C_{23}- δD	C_{27}- δD	C_{29}- δD	C_{31}- δD	C_{33}- δD	C_{35}- δD	$\varepsilon_{(terr\text{-}aq)}$	Phase
17,038	n/a	−137	−142	−151	−141	−144	n/a	TQ6
17,345	−127	−123	−140	−152	−148	−149	−14	TQ6
17,655	−144	−143	−151	−159	−156	−146	−8	TQ6
17,965	−148	−138	−149	−157	−154	−156	−1	TQ6
23,522	−124	n/a	−144	n/a	n/a	n/a	−22	TP2
23,706	−114	−124	−135	−153	−137	−140	−23	TP2
24,447	−123	−132	−145	−155	−157	−155	−25	TP2
25,519	−136	−133	−151	−157	−149	−148	−17	TP2
27,716	−149	−138	−151	−161	−163	−162	−2	TQ7
27,925	−146	−132	−148	−158	−161	−163	−2	TQ7
28,030	−140	−134	−148	−158	−158	−160	−9	TQ7
28,134	−144	−136	−149	−156	−158	−158	−5	TQ7
29,693	−116	−136	−145	−153	−149	−156	−32	TP3
30,075	−120	−130	−141	−151	−143	−138	−23	TP3
30,457	−129	−138	−145	−151	−146	−149	−17	TP3
31,804	−129	−139	−145	−157	−155	−143	−18	TP3
35,511	−158	−135	−156	−169	−170	−164	2	TQ8
36,068	−149	−132	−155	−170	−169	n/a	−7	TQ8
36,207	−153	−140	−155	−166	−168	−158	−2	TQ8
36,347	−143	−143	−151	−168	−167	−156	−9	TQ8
37,180	−124	−131	−152	−159	−161	−156	−32	TP4
38,014	−123	−135	−143	−155	−148	−150	−22	TP4
39,386	−131	−137	−147	−162	−165	−160	−18	TP4
39,923	−129	−135	−144	−161	−156	−150	−17	TP4

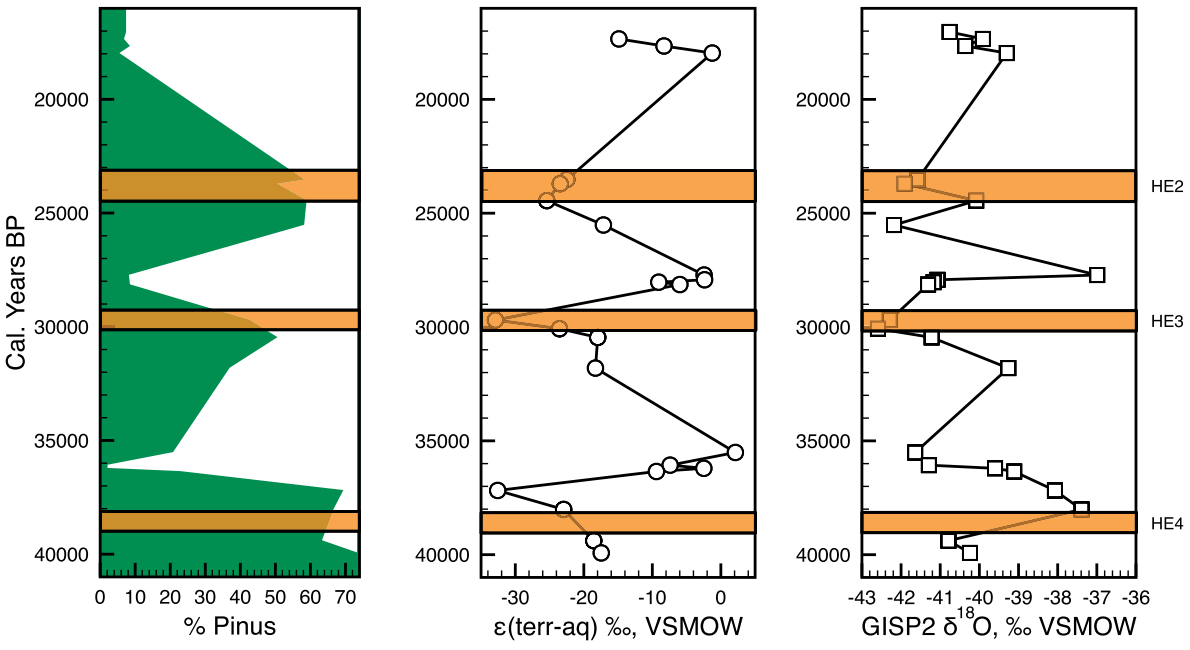

Fig. 4. Pinus pollen abundances (first column), $\varepsilon_{(terr\text{-}aq)}$ values (second column), and GISP2 $\delta^{18}O$ values taken from Stuiver and Grootes (2000) (third column). Heinrich Event ages (HE 4-2) are taken from Stoner et al. (2000) and are outlined with orange bars. The $\varepsilon_{(terr\text{-}aq)}$ values are calculated from the difference of δD values in (A) and (B), and are essentially an approximation of aridity, with higher values indicating more arid conditions. The pooled 1σ SE for all samples was ±3.2‰. (For interpretation of the references to colour in this figure legend, the reader is referred to the Web version of this article.)

during *Quercus* zones.

The *n*-C_{29} data can thus be classified as a terrestrial C_3 angiosperm biomarker. The two dominant angiosperms in the Lake Tulane pollen record, *Quercus* and *Ambrosia* account for ~50% of all pollen recorded during interstadials, and 10–25% during stadials. Carbon isotope ratios measured in *n*-C_{29} alkanes from three species of *Quercus* returned values ranging from 33.3‰ to 34.8‰ (Chikaraishi and Naraoka, 2003), and bulk $\delta^{13}C$ measurements on individual *Q. chrysolepis* from a single study site ranged from −30‰ to −27‰ (Feakins and Sessions, 2010). Therefore, the *n*-C_{29} Δ_{leaf} record can reasonably be interpreted as a record of changes in water availability. The relatively strong correlation between *Pinus* pollen relative abundance and *n*-C_{29} Δ_{leaf} values indicates that water availability certainly changed as the climate system in the northern hemisphere responded to HE.

To complement carbon isotope data, we analyzed hydrogen isotope ratios in aquatic (*n*-C_{23}) and terrestrial lipids (*n*-C_{29}) (Fig. 3). *n*-C_{23} is produced by multiple plant types, but submerged aquatic

macrophytes tend to produce a greater relative abundance than terrestrial plants and algae (Ficken et al., 2000; Aichner et al., 2010a; Diefendorf et al., 2011; Gao et al., 2011; Diefendorf and Freimuth, 2017). The δD values of n-C_{23} reflect variability in δD_{lake}, but could also reflect changes in biosynthetic fractionation, which is assumed to be constant (Sachse et al., 2012; Rach et al., 2014, 2017). Because Lake Tulane is a small catchment system without major inflows or evaporative isotope effects, δD_{lake} values can be used as a proxy for the δD of mean annual precipitation (e.g., Rach et al., 2017). Isotope values of δD_{terr} track precipitation, but are also influenced by biosynthetic fractionation and fractionation that occurs during soil and leaf water evaporation (Smith and Freeman, 2006; Sachse et al., 2012; Kahmen et al., 2013a; b). By calculating the fractionation between δD_{terr} and δD_{lake} ($\varepsilon_{(terr\text{-}aq)}$, Eq. (7)), it should be possible to track the relative change aridity through time at Lake Tulane (e.g., Rach et al., 2014; Rach et al., 2017). On average, the values for our aridity proxy decrease by 17‰ during *Pinus* phases. These results are in line with model simulations that produce deuterium enrichment in n-alkanes by as much as 10–30‰ during evapotranspiration in temperate environments (Kahmen et al., 2013b). The negative correlation between $\varepsilon_{(terr\text{-}aq)}$ and *Pinus* pollen percentages ($r = -0.80$, $p < 0.001$) (Fig. 4) identifies these as zones of lower isotopic enrichment and thus lower aridity. This would suggest that *Pinus* proliferated during these wetter periods associated with HE.

The $\varepsilon_{(terr\text{-}aq)}$ and Δ_{leaf} values should correlate with one another because both are indicators of aridity, however, the correlation coefficient between the two variables is below 0.2 ($p = 0.8$). A possible explanation for this discrepancy lies in the variable sources of carbon and hydrogen isotopes to the plant leaves. Whereas $\varepsilon_{(terr\text{-}aq)}$ values record changes in the source of precipitation and the effects of aridity, Δ_{leaf} values are only affected by aridity. Changes in precipitation isotopes would, therefore, only be recorded in the hydrogen isotopic signature, making the weak correlation between the two, not entirely unexpected.

4.2. Tracking paleo-precipitation using hydrogen isotopes of aquatic vegetation

Paleo-precipitation isotope values, estimated from δD_{lake} values, decrease by an average of 22‰ during *Quercus* periods (Fig. 3). The simplest explanation for this decrease in δD_{lake} values invokes lower air temperature in the subtropics during Greenland interstadials (Gat, 1996). Lower temperatures reduce δD_{lake} values of precipitation by lowering the amount of water retained in a given air mass (Fricke and O'Neil, 1999). However, invoking air temperature as the primary driver of our δD_{lake} record is problematic because: 1) the correlation between the condensation temperature and $\delta D_{precipitation}$ values is valid only in temperate climates (Alley and Cuffey, 2001) and, 2) isotope fractionation results from a latitudinal displacement of the vapor source. Although Florida and other subtropical sites were colder or more temperate during the last glacial period (Hodell et al., 2012), the majority of the precipitation in the study region came from rapidly cooling convective storm systems that would have resulted in only minimal Rayleigh distillation (Grimm et al., 2006).

Stadial *(Pinus)* and interstadial (*Quercus)* zones can be differentiated on the basis of AMOC strength. Reduced AMOC strength during cold stadials in the North Atlantic results in higher SST and expansion of the Atlantic Warm Pool around peninsular Florida (Dahl et al., 2005; Donders et al., 2011). Resumption of normal AMOC flow during interstadials has been linked to reduced SSTs in the Gulf of Mexico (Carlson et al., 2008) and cooler ocean temperatures. Other studies have demonstrated a strong correlation between decreased SST in the equatorial North Atlantic and more southward position of the Inter-tropical Convergence Zone (ITCZ) (Hodell et al., 1991; Poore et al., 2003). Whereas a warm Gulf of Mexico would ultimately increase convective storm activity around the peninsula, a southern displacement of the ITCZ would bring more frontal systems to Florida because of increased westerly storm tracks (Van Soelen et al., 2012). These two storm systems would be isotopically distinct: frontal storms would undergo more substantial Rayleigh distillation, whereas convective systems would not. We speculate that during interstadials (*Quercus* zones) lower atmospheric temperatures and greater frontal precipitation resulted in lower δD_{lake} and precipitation values relative to stadials (*Pinus* zones).

4.3. Implications of rapid climate change events in the subtropics

Carbon and hydrogen isotopes from n-C_{29} and n-C_{23} alkanes indicate that aridity decreased, and atmospheric temperatures increased at Lake Tulane during *Pinus* phases at Lake Tulane and HE/Greenland stadials. The Lake Tulane pollen record from Grimm et al. (2006) for the Lake Tulane sequence showed an apparent inverse correlation between temperatures in Greenland and south-central Florida. Multiple reconstructions of SST during HE indicate that surface waters south of the ice-rafted debris belt warmed as temperatures over Greenland dropped (Flower et al., 2004; Schmidt et al., 2006; Weldeab et al., 2006), and temperature in the Gulf of Mexico also remained warm throughout Greenland stadials, implying persistence of the Atlantic Warm Pool around peninsular Florida (Carlson et al., 2008; Ziegler et al., 2008; Rasmussen and Thomsen, 2012). But what could have kept Florida and the Gulf of Mexico warm and wet during the extreme cold events in the North Atlantic? Results of pollen-based climate inference models (Donders et al., 2011) link a warm, persistent Atlantic Warm Pool with northward displacement of the ITCZ and increased precipitation across the Florida Peninsula during cold periods in the high-latitude North Atlantic. Today, the source and seasonal delivery of precipitation in Florida is similar to that in the late Pleistocene (Grimm et al., 2006; Donders et al., 2011). Northward displacement of the ITCZ during boreal summer increases southeasterly trade wind strength over the subtropical North Atlantic, resulting in greater rainfall on the peninsula. Other studies showed that during Greenland stadials, the southward displacement of the polar front was associated with an expansion of the subpolar gyre and a westward movement of the subtropical gyre (Eynaud et al., 2009). The westward shift of the subtropical gyre results in a narrower Gulf Stream and moves it closer to the continent (Hoogakker et al., 2013). This agrees with inferred stadial/interstadial shifts in the position of the Gulf Stream (Hoogakker et al., 2013), and warmer mid-latitude North Atlantic SSTs during stadial periods (Naafs et al., 2013). A narrower Gulf Stream, located closer to the Florida Peninsula, would have reduced northward heat transport, and could explain why Florida remained warm and relatively wet during the Heinrich stadials.

Data from multiple studies (e.g. Kreveld et al., 2000) indicate that the duration and magnitude of the climate system response to HE6-1 was not uniform. Our $\varepsilon_{(terr\text{-}aq)}$ record spans a range of 36‰ and records multiple abrupt shifts in aridity. During HE4-3, departures towards more negative $\varepsilon_{(terr\text{-}aq)}$ values indicate that these HE elicited the strongest response from the hydrological cycle, whereas HE2 produced a more muted response. It is not surprising that HE4 resulted in the largest shift toward less arid values, as it was the largest of the six HE in terms of % ice-rafted debris (Hemming, 2004; Tierney et al., 2008). The subdued response in our hydrogen isotope record during HE2 is also expected, as studies have demonstrated that there was no reduction in AMOC intensity across that interval (Lynch-Stieglitz et al., 2014; Parker et al., 2015).

The pronounced response during HE3, however, does not match sediment data that classify it as a "low-foraminifera interval", with limited change in AMOC strength, rather than a true ice-rafting event (Hemming, 2004; Lynch-Stieglitz et al., 2014). Tulane *Pinus* zone 3, which correlates to HE3, has lower abundances of *Pinus* pollen and higher abundances of *Ambrosia* than *Pinus* zones 1, 4, 5, and 6, suggesting cooler temperatures during HE3 (Grimm et al., 2006). If HE3 was not caused by a reduction in AMOC strength associated with freshening of the North Atlantic, another, as yet unidentified mechanism is needed to explain the hydrological changes during HE3. It is possible that ITCZ position and attendant atmospheric teleconnections remained similar during all six HE, even if the AMOC strength and sediment ice-rafted debris percentages varied.

The fact that both temperature and precipitation at Lake Tulane responded in concert with rapid climatic variability in the high-latitude Northern Hemisphere demonstrates that glacial calving events have a strong influence on climate in the subtropics. Although these events produce cooling and drying throughout much of the Northern Hemisphere, it is apparent that this was not the case in peninsular Florida. The antiphase relationship underscores the complex teleconnections that link atmospheric temperatures with oceanic SSTs and circulation patterns. The reduction in AMOC strength limited the amount of thermal energy that could be redistributed to the poles but resulted in the persistence of the Atlantic Warm Pool and intensification of ocean currents and trade winds in the low-latitude North Atlantic, which increased atmospheric temperatures and precipitation. Atmospheric warming is seen in other terrestrial records (e.g. Tierney et al., 2008) during HE, however warming never coincided with decreased aridity. Thus, responses to rapid climate change events are regional and may differ, and depending on myriad factors, including, but not limited to: SST gradients, latent heat fluxes, and circulation patterns that influence regional atmospheric circulation patterns.

5. Conclusions

We inferred a record of past climate and environmental change preserved in sediments from Lake Tulane, Florida, which were deposited across HE 2-4. Δ_{leaf} values measured from leaf wax showed the effects of variable aridity regimes: higher Δ_{leaf} values during the wetter *Pinus* periods and lower Δ_{leaf} values during the drier *Quercus* periods. We interpret shifts in aquatic δD_{lipid} values to represent changes in both condensation temperature and storm pathway, with higher δD values during *Pinus* periods resulting from warmer temperatures and localized convective storm activity. Terrestrial δD_{lipid} values were paired with aquatic δD_{lipid} values to estimate aridity changes across HE and intervening interstadials. These $\varepsilon_{(terr\text{-}aq)}$ values correlate strongly with *Pinus* pollen relative abundance, and, like the Δ_{leaf} values, signify less arid conditions during *Pinus* phases. Taken together, our results demonstrate that temperatures on the Florida Peninsula were out of phase with those at high latitudes during at least three of the late Pleistocene stadial-interstadial transitions. The Florida region remained warm and wet during stadials, likely due to reduced northward export of warm, saline water from the subtropical Atlantic Ocean.

Acknowledgements

We thank Erika Freimuth and Laurie Eccles for assistance with δD and $\delta^{13}C$ analyses. Portions of the research were supported by the US National Science Foundation (EAR-1229114 to AFD) and the Inter-University Training in Continental-scale Ecology (ITCE Project) Award Numbers EF-1137336 and EF-1240142 from the National Science Foundation.

References

Aichner, B., Herzschuh, U., Wilkes, H., 2010a. Influence of aquatic macrophytes on the stable carbon isotopic signatures of sedimentary organic matter in lakes on the Tibetan Plateau. Org. Geochem. 41 (7), 706–718.
Aichner, B., Herzschuh, U., Wilkes, H., Vieth, A., Böhner, J., 2010b. äD values of n-alkanes in Tibetan lake sediments and aquatic macrophytes–A surface sediment study and application to a 16 ka record from Lake Koucha. Org. Geochem. 41 (8), 779–790.
Alley, R.B., Cuffey, K.M., 2001. Oxygen-and hydrogen-isotopic ratios of water in precipitation: beyond paleothermometry. Rev. Mineral. Geochem. 43 (1), 527–553.
Bennett, K.D., Willis, K.J., 2002. Pollen. In Tracking Environmental Change Using lake Sediments. Springer, Netherlands, pp. 5–32.
Bond, G., Broecker, W., Johnsen, S., McManus, J., Labeyrie, L., Jouzel, J., Bonani, G., 1993. Correlations between climate records from North Atlantic sediments and Greenland ice. Nature 365 (6442), 143–147.
Broecker, W., Bond, G., Klas, M., Clark, E., McManus, J., 1992. Origin of the northern Atlantic's Heinrich events. Clim. Dynam. 6 (3–4), 265–273.
Broecker, W.S., 2006. Abrupt climate change revisited. Global Planet. Change 54 (3), 211–215.
Cacho, I., Grimalt, J.O., Pelejero, C., Canals, M., Sierro, F.J., Flores, J.A., Shackleton, N., 1999. Dansgaard-oeschger and Heinrich event imprints in Alboran sea paleotemperatures. Paleoceanography 14 (6), 698–705.
Carlson, A.E., Oppo, D.W., Came, R.E., LeGrande, A.N., Keigwin, L.D., Curry, W.B., 2008. Subtropical Atlantic salinity variability and Atlantic meridional circulation during the last deglaciation. Geology 36 (12), 991–994.
Chikaraishi, Y., Naraoka, H., 2003. Compound-specific δD–$\delta^{13}C$ analyses of n-alkanes extracted from terrestrial and aquatic plants. Phytochemistry 63 (3), 361–371.
Dahl, K.A., Broccoli, A.J., Stouffer, R.J., 2005. Assessing the role of North Atlantic freshwater forcing in millennial scale climate variability: a tropical Atlantic perspective. Clim. Dynam. 24 (4), 325–346.
Diefendorf, A.F., Mueller, K.E., Wing, S.L., Koch, P.L., Freeman, K.H., 2010. Global patterns in leaf ^{13}C discrimination and implications for studies of past and future climate. Proc. Natl. Acad. Sci. Unit. States Am. 107 (13), 5738–5743.
Diefendorf, A.F., Freeman, K.H., Wing, S.L., Graham, H.V., 2011. Production of n-alkyl lipids in living plants and implications for the geologic past. Geochem. Cosmochim. Acta 75 (23), 7472–7485.
Diefendorf, A.F., Leslie, A.B., Wing, S.L., 2015. Leaf wax composition and carbon isotopes vary among major conifer groups. Geochem. Cosmochim. Acta 170, 145–156.
Diefendorf, A.F., Freimuth, E.J., 2017. Extracting the most from terrestrial plant-derived n-alkyl lipids and their carbon isotopes from the sedimentary record: a review. Org. Geochem. 103, 1–21.
Donders, T.H., de Boer, H.J., Finsinger, W., Grimm, E.C., Dekker, S.C., Reichart, G.J., Wagner-Cremer, F., 2011. Impact of the Atlantic warm pool on precipitation and temperature in Florida during North Atlantic cold spells. Clim. Dynam. 36 (1–2), 109–118.
Douglas, P.M., Pagani, M., Brenner, M., Hodell, D.A., Curtis, J.H., 2012. Aridity and vegetation composition are important determinants of leaf-wax δD values in southeastern Mexico and Central America. Geochem. Cosmochim. Acta 97, 24–45.
Eggleston, S., Schmitt, J., Bereiter, B., Schneider, R., Fischer, H., 2016. Evolution of the stable carbon isotope composition of atmospheric CO_2 over the last glacial cycle. Paleoceanography 31 (3), 434–452.
Eglinton, G., Hamilton, R.J., 1967. Leaf epicuticular waxes. Science 156 (3780), 1322–1335.
Ehleringer, J.R., Cooper, T.A., 1988. Correlations between carbon isotope ratio and microhabitat in desert plants. Oecologia 76 (4), 562–566.
Escobar, J., Buck, D.G., Brenner, M., Curtis, J.H., Hoyos, N., 2009. Thermal stratification, mixing, and heat budgets of Florida lakes. Fundamental and Applied Limnology/Archiv für Hydrobiologie 174 (4), 283–293.
Eynaud, F., De Abreu, L., Voelker, A., Schönfeld, J., Salgueiro, E., Turon, J.L., et al., 2009. Position of the Polar Front along the western Iberian margin during key cold episodes of the last 45 ka. G-cubed 10 (7).
Fairbanks, R.G., Mortlock, R.A., Chiu, T.C., Cao, L., Kaplan, A., Guilderson, T.P., et al., 2005. Radiocarbon calibration curve spanning 0 to 50,000 years BP based on paired $^{230}Th/^{234}U/^{238}U$ and ^{14}C dates on pristine corals. Quat. Sci. Rev. 24 (16), 1781–1796.
Farquhar, G.D., Ehleringer, J.R., Hubick, K.T., 1989. Carbon isotope discrimination and photosynthesis. Annu. Rev. Plant Biol. 40 (1), 503–537.
Feakins, S.J., Sessions, A.L., 2010. Controls on the D/H ratios of plant leaf waxes in an arid ecosystem. Geochem. Cosmochim. Acta 74 (7), 2128–2141.
Ferrio, J.P., Voltas, J., Araus, J.L., 2003. Use of carbon isotope composition in monitoring environmental changes. Manag. Environ. Qual. Int. J. 14 (1), 82–98.
Ficken, K.J., Li, B., Swain, D.L., Eglinton, G., 2000. An n-alkane proxy for the sedimentary input of submerged/floating freshwater aquatic macrophytes. Org. Geochem. 31 (7), 745–749.
Flower, B.P., Hastings, D.W., Hill, H.W., Quinn, T.M., 2004. Phasing of deglacial warming and laurentide ice sheet meltwater in the Gulf of Mexico. Geology 32 (7), 597–600.

Florea, L.J., McGee, D.K., 2010. Stable isotopic and geochemical variability within shallow groundwater beneath a hardwood hammock and surface water in an adjoining slough (Everglades National Park, Florida, USA). Isot. Environ. Health Stud. 46 (2), 190–209.
Freimuth, E.J., Diefendorf, A.F., Lowell, T.V., 2017. Hydrogen isotopes of n-alkanes and n-alkanoic acids as tracers of precipitation in a temperate forest and implications for paleorecords. Geochem. Cosmochim. Acta 206, 166–183.
Fricke, H.C., O'Neil, J.R., 1999. The correlation between 18O/16O ratios of meteoric water and surface temperature: its use in investigating terrestrial climate change over geologic time. Earth Planet Sci. Lett. 170 (3), 181–196.
Gao, L., Hou, J., Toney, J., MacDonald, D., Huang, Y., 2011. Mathematical modeling of the aquatic macrophyte inputs of mid-chain n-alkyl lipids to lake sediments: implications for interpreting compound specific hydrogen isotopic records. Geochem. Cosmochim. Acta 75 (13), 3781–3791.
Garcin, Y., Schefuß, E., Schwab, V.F., Garreta, V., Gleixner, G., Vincens, A., et al., 2014. Reconstructing C_3 and C_4 vegetation cover using n-alkane carbon isotope ratios in recent lake sediments from Cameroon, Western Central Africa. Geochem. Cosmochim. Acta 142, 482–500.
Gat, J.R., 1996. Oxygen and hydrogen isotopes in the hydrologic cycle. Annu. Rev. Earth Planet Sci. 24 (1), 225–262.
Grimm, E.C., Jacobson, G.L., Watts, W.A., Hansen, B.C., Maasch, K.A., 1993. A 50,000-year record of climate oscillations from Florida and its temporal correlation with the Heinrich events. Science-New York Then Washington- 261, 198.
Grimm, E.C., Watts, W.A., Jacobson, G.L., Hansen, B.C., Almquist, H.R., Dieffenbacher-Krall, A.C., 2006. Evidence for warm wet Heinrich events in Florida. Quat. Sci. Rev. 25 (17), 2197–2211.
Hartman, G., Danin, A., 2010. Isotopic values of plants in relation to water availability in the Eastern Mediterranean region. Oecologia 162 (4), 837–852.
Hemming, S.R., 2004. Heinrich events: massive late Pleistocene detritus layers of the North Atlantic and their global climate imprint. Rev. Geophys. 42 (1).
Hodell, D.A., Curtis, J.H., Jones, G.A., Higuera-Gundy, A., Brenner, M., Binford, M.W., Dorsey, K.T., 1991. Reconstruction of Caribbean climate change over the past 10,500 years. Nature 352 (6338), 790.
Hodell, D.A., Turchyn, A.V., Wiseman, C.J., Escobar, J., Curtis, J.H., Brenner, M., et al., 2012. Late Glacial temperature and precipitation changes in the lowland Neotropics by tandem measurement of $\delta^{18}O$ in biogenic carbonate and gypsum hydration water. Geochem. Cosmochim. Acta 77, 352–368.
Hoogakker, B.A.A., Downy, F., Andersson, M.A., Chapman, M.R., Elderfield, H., McCave, I.N., et al., 2013. Gulf Stream–subtropical gyre properties across two Dansgaard–Oeschger cycles. Quat. Sci. Rev. 81, 105–113.
Huang, Y., Shuman, B., Wang, Y., Webb, T., Grimm, E.C., Jacobson, G.L., 2006. Climatic and environmental controls on the variation of C_3 and C_4 plant abundances in central Florida for the past 62,000 years. Palaeogeogr. Palaeoclimatol. Palaeoecol. 237 (2), 428–435.
Jacob, J., Huang, Y., Disnar, J.R., Sifeddine, A., Boussafir, M., Albuquerque, A.L.S., Turcq, B., 2007. Paleohydrological changes during the last deglaciation in Northern Brazil. Quat. Sci. Rev. 26 (7–8), 1004–1015.
Kahmen, A., Simonin, K., Tu, K.P., Merchant, A., Callister, A., Siegwolf, R., et al., 2008. Effects of environmental parameters, leaf physiological properties and leaf water relations on leaf water $\delta^{18}O$ enrichment in different Eucalyptus species. Plant Cell Environ. 31 (6), 738–751.
Kahmen, A., Schefuß, E., Sachse, D., 2013a. Leaf water deuterium enrichment shapes leaf wax *n*-alkane δD values of angiosperm plants I: experimental evidence and mechanistic insights. Geochem. Cosmochim. Acta 111, 39–49.
Kahmen, A., Hoffmann, B., Schefuß, E., Arndt, S.K., Cernusak, L.A., West, J.B., Sachse, D., 2013b. Leaf water deuterium enrichment shapes leaf wax *n*-alkane δD values of angiosperm plants II: observational evidence and global implications. Geochem. Cosmochim. Acta 111, 50–63.
Kohn, M.J., 2010. Carbon isotope compositions of terrestrial C_3 plants as indicators of (paleo) ecology and (paleo) climate. Proc. Natl. Acad. Sci. Unit. States Am. 107 (46), 19691–19695.
Kreveld, S.V., Sarnthein, M., Erlenkeuser, H., Grootes, P., Jung, S., Nadeau, M.J., et al., 2000. Potential links between surging ice sheets, circulation changes, and the Dansgaard-Oeschger cycles in the Irminger Sea, 60–18 kyr. Paleoceanography 15 (4), 425–442.
Leuenberger, M., Siegenthaler, U., Langway, C., 1992. Carbon isotope composition of atmospheric CO_2 during the last ice age from an Antarctic ice core. Nature 357 (6378), 488–490.
Lynch-Stieglitz, J., Schmidt, M.W., Henry, L.G., Curry, W.B., Skinner, L.C., Mulitza, S., et al., 2014. Muted change in Atlantic overturning circulation over some glacial-aged Heinrich events. Nat. Geosci. 7 (2), 144–150.
Magill, C.R., Ashley, G.M., Freeman, K.H., 2013. Water, plants, and early human habitats in eastern Africa. Proc. Natl. Acad. Sci. Unit. States Am. 110 (4), 1175–1180.
Marcott, S.A., Clark, P.U., Padman, L., Klinkhammer, G.P., Springer, S.R., Liu, Z., et al., 2011. Ice-shelf collapse from subsurface warming as a trigger for Heinrich events. Proc. Natl. Acad. Sci. Unit. States Am. 108 (33), 13415–13419.
Marzi, R., Torkelson, B.E., Olson, R.K., 1993. A revised carbon preference index. Org. Geochem. 20 (8), 1303–1306.
Naafs, B.D.A., Hefter, J., Gruetzner, J., Stein, R., 2013. Warming of surface waters in the mid-latitude North Atlantic during Heinrich events. Paleoceanography 28 (1), 153–163.
Nichols, J.E., 2011. Procedures for extraction and purification of leaf wax biomarkers from peats. Mires Peat 7 (13), 1–7.
Pailler, D., Bard, E., 2002. High frequency palaeoceanographic changes during the past 140,000 yr recorded by the organic matter in sediments of the Iberian Margin. Palaeogeogr. Palaeoclimatol. Palaeoecol. 181 (4), 431–452.
Parker, A.O., Schmidt, M.W., Chang, P., 2015. tropical North Atlantic subsurface warming events as a fingerprint for AMOC variability during marine isotope stage 3. Paleoceanography 30 (11), 1425–1436.
Patton, G.M., Martin, P.A., Voelker, A., Salgueiro, E., 2011. Multiproxy comparison of oceanographic temperature during Heinrich Events in the eastern subtropical Atlantic. Earth Planet Sci. Lett. 310 (1), 45–58.
Polissar, P.J., Freeman, K.H., 2010. Effects of aridity and vegetation on plant-wax δD in modern lake sediments. Geochem. Cosmochim. Acta 74 (20), 5785–5797.
Polissar, P.J., D'Andrea, W.J., 2014. Uncertainty in paleohydrologic reconstructions from molecular δD values. Geochem. Cosmochim. Acta 129, 146–156.
Poore, R.Z., Dowsett, H.J., Verardo, S., Quinn, T.M., 2003. Millennial-to century-scale variability in Gulf of Mexico Holocene climate records. Paleoceanography 18 (2).
Rach, O., Brauer, A., Wilkes, H., Sachse, D., 2014. Delayed hydrological response to Greenland cooling at the onset of the Younger Dryas in western Europe. Nat. Geosci. 7 (2), 109–112.
Rach, O., Kahmen, A., Brauer, A., Sachse, D., 2017. A dual-biomarker approach for quantification of changes in relative humidity from sedimentary lipid D/ H ratios. Clim. Past 13 (7), 741.
Rasmussen, T.L., Thomsen, E., 2012. Changes in planktic foraminiferal faunas, temperature and salinity in the Gulf Stream during the last 30,000 years: influence of meltwater via the Mississippi River. Quat. Sci. Rev. 33, 42–54.
Renold, M., Raible, C.C., Yoshimori, M., Stocker, T.F., 2010. Simulated resumption of the North Atlantic meridional overturning circulation–Slow basin-wide advection and abrupt local convection. Quat. Sci. Rev. 29 (1), 101–112.
Sachse, D., Radke, J., Gleixner, G., 2004. Hydrogen isotope ratios of recent lacustrine sedimentary *n*-alkanes record modern climate variability. Geochem. Cosmochim. Acta 68 (23), 4877–4889.
Sachse, D., Gleixner, G., Wilkes, H., Kahmen, A., 2010. Leaf wax *n*-alkane δD values of field-grown barley reflect leaf water δD values at the time of leaf formation. Geochem. Cosmochim. Acta 74 (23), 6741–6750.
Sachse, D., Billault, I., Bowen, G.J., Chikaraishi, Y., Dawson, T.E., Feakins, S.J., et al., 2012. Molecular paleohydrology: interpreting the hydrogen-isotopic composition of lipid biomarkers from photosynthesizing organisms. Annu. Rev. Earth Planet Sci. 40, 221–249.
Schmidt, M.W., Vautravers, M.J., Spero, H.J., 2006. Rapid subtropical North Atlantic salinity oscillations across dansgaard–oeschger cycles. Nature 443 (7111), 561–564.
Schubert, B.A., Jahren, A.H., 2012. The effect of atmospheric CO_2 concentration on carbon isotope fractionation in C_3 land plants. Geochem. Cosmochim. Acta 96, 29–43.
Smith, F.A., Freeman, K.H., 2006. Influence of physiology and climate on δD of leaf wax *n*-alkanes from C_3 and C_4 grasses. Geochem. Cosmochim. Acta 70, 1172–1187.
Stewart, G.R., Turnbull, M.H., Schmidt, S., Erskine, P.D., 1995. ^{13}C natural abundance in plant communities along a rainfall gradient: a biological integrator of water availability. Funct. Plant Biol. 22 (1), 51–55.
Stoner, J.S., Channell, J.E.T., Hillaire-Marcel, C., Kissel, C., 2000. Geomagnetic paleointensity and environmental record from Labrador Sea core MD95-2024: global marine sediment and ice core chronostratigraphy for the last 110 kyr. Earth Planet Sci. Lett. 183 (1), 161–177.
Stuiver, M., Grootes, P.M., 2000. GISP2 oxygen isotope ratios. Quat. Res. 53 (3), 277–284.
Tierney, J.E., Russell, J.M., Huang, Y., Damsté, J.S.S., Hopmans, E.C., Cohen, A.S., 2008. Northern hemisphere controls on tropical southeast African climate during the past 60,000 years. Science 322 (5899), 252–255.
Van Soelen, E.E., Brooks, G.R., Larson, R.A., Sinninghe Damsté, J.S., Reichart, G.J., 2012. Mid-to late-Holocene coastal environmental changes in southwest Florida, USA. Holocene 22 (8), 929–938.
Waghorn, M.J., Whitehead, D., Watt, M.S., Mason, E.G., Harrington, J.J., 2015. Growth, biomass, leaf area and water-use efficiency of juvenile *Pinus radiata* in response to water deficits. New Zealand Journal of Forestry Science 45 (1), 3.
Wang, Y.V., Larsen, T., Leduc, G., Andersen, N., Blanz, T., Schneider, R.R., 2013. What does leaf wax δD from a mixed C_3/C_4 vegetation region tell us? Geochem. Cosmochim. Acta 111, 128–139.
Weaver, A.J., Saenko, O.A., Clark, P.U., Mitrovica, J.X., 2003. Meltwater pulse 1A from Antarctica as a trigger of the Bølling-Allerød warm interval. Science 299 (5613), 1709–1713.
Weldeab, S., Schneider, R.R., Kölling, M., 2006. Deglacial sea surface temperature and salinity increase in the western tropical Atlantic in synchrony with high latitude climate instabilities. Earth Planet Sci. Lett. 241 (3), 699–706.
White, W.A., 1970. The geomorphology of the Florida peninsula. GSA Bulletin 51, 1–172.
Zhao, J.X., Wang, Y.J., Collerson, K.D., Gagan, M.K., 2003. Speleothem U-series dating of semi-synchronous climate oscillations during the last deglaciation. Earth Planet Sci. Lett. 216 (1), 155–161.
Zhou, H., Zhao, J., Feng, Y., Gagan, M.K., Zhou, G., Yan, J., 2008. Distinct climate change synchronous with Heinrich event one, recorded by stable oxygen and carbon isotopic compositions in stalagmites from China. Quat. Res. 69 (2), 306–315.
Ziegler, M., Nürnberg, D., Karas, C., Tiedemann, R., Lourens, L.J., 2008. Persistent summer expansion of the Atlantic Warm Pool during glacial abrupt cold events. Nat. Geosci. 1 (9), 601–605.